

Structural and energetic properties of domains in PbTiO₃/SrTiO₃ superlattices from first principles

Pablo Aguado-Puente and Javier Junquera

Departamento de Ciencias de la Tierra y Física de la Materia Condensada, Universidad de Cantabria, Cantabria Campus Internacional, Avenida de los Castros s/n, 39005 Santander, Spain

(Received 24 February 2012; published 16 May 2012)

We report first-principles calculations, within the density functional theory, on the structural and energetic properties of 180° stripe domains in (PbTiO₃)_n/(SrTiO₃)_n superlattices. For the explored periodicities ($n = 3$ and 6), we find that the polydomain structures compete in energy with the monodomain phases. Our results suggest the progressive transition, as a function of n , from a strong to a weak electrostatic coupling regime between the SrTiO₃ and PbTiO₃ layers. Structurally, they display continuous rotation of polarization connecting 180° domains. A large offset between [100] atomic rows across the domain wall and huge strain gradients are observed. The domain wall energy is very isotropic, depending very weakly on the stripe orientation.

DOI: [10.1103/PhysRevB.85.184105](https://doi.org/10.1103/PhysRevB.85.184105)

PACS number(s): 77.55.Px, 77.80.Dj, 77.80.bn, 77.84.Cg

I. INTRODUCTION

The growth of superlattices composed of thin layers of ABO₃ perovskites with different physical properties has become one of the most promising paths to exploit the coupling between instabilities in order to engineer new functionalities in these heterostructures.^{1–3} For a long time the focus was on the electrostatic coupling between the layers of the superlattice,^{4,5} and the interplay with the epitaxial strain.⁶ More recently, after the discovery of the appearance of a polarization from the coupling of two rotational modes in ultrashort period PbTiO₃/SrTiO₃ superlattices,⁷ the interest has evolved to include also the interaction between ferroelectric (FE) and antiferrodistortive (AFD) modes in perovskite related layered compounds.^{8–10}

At the same time, polarization domains in ferroelectric thin films are being subject of numerous investigations due to the recent finding of their intrinsic functional properties. One of the most remarkable is the conductivity at domain walls within an otherwise insulating material.^{11,12} The great activity in the research of polydomain phases in ferroelectric thin films has also demonstrated that the domain structure in these systems, with rotation of the polarization^{13,14} or the formation of flux-closure structures in thin films,^{15–20} and vortex structures in nanosized ferroelectrics,^{21,22} probably differs significantly from the typically assumed picture of alternating regions where the polarization points along opposite directions with sharp domain walls (DW).

In the particular case of PbTiO₃/SrTiO₃ interfaces, pioneer works were devoted to the identification of 180° stripe domains in PbTiO₃ *thin films* grown on thick SrTiO₃ (001) substrates. The domain structures were characterized both in reciprocal space (strong satellites around PbTiO₃ Bragg peaks in synchrotron x-ray scattering measurements),^{23–25} and in real space (images recorded by atomic force microscopy).²⁶ Only lately, the attention has turned to the study of the domain structures in PbTiO₃/SrTiO₃ *superlattices*. Zubko and coworkers²⁷ have recently focused on the dependence of their structural and dielectric properties as a function of the volume fraction of PbTiO₃, the electrodes, and the applied electric fields. While the results of the superlattices asymmetrically sandwiched between Nb-doped SrTiO₃ (bottom) and gold (top) electrodes were consistent with a monodomain configuration,²⁸ those

corresponding to the use of symmetrically coated SrRuO₃ electrodes (both top and bottom) suggested a polydomain phase with DW motion, which dynamics might be quite different than the conventional one.²⁹ Furthermore, through a combination of x-ray diffraction, transmission electron microscopy, and ultrahigh resolution electron energy loss spectroscopy (EELS), Zubko *et al.*^{30,31} have also recently showed the progressive transition between two different regimes, controlled by the thickness of the individual SrTiO₃ and PbTiO₃ layers. In the first regime, present for sufficiently thin paraelectric layers, SrTiO₃ and PbTiO₃ are strongly electrostatically *coupled*: a uniform monodomain polarization is adopted throughout the thickness of the superlattice to minimize the depolarizing field. In the second regime, when the paraelectric layer thickness is increased, SrTiO₃ and PbTiO₃ are *decoupled*: the polarization is confined within the FE PbTiO₃ layers forming domains. EELS measurements revealed the presence of broad interfacial layers with reduced tetragonality and polarization extending over 5–6 unit cells (u.c.) into the PbTiO₃ layers. Strikingly, in the electrostatic decoupled regime, the domain structure was found to be coherent over several tens of superlattice repetitions. These works pointed out the suitability of this system for the study of domains in ultrathin ferroelectric films, given the behavior of the ferroelectric layers as quasi-independent films, while the thickness of the whole system prevents the charge leakage when electric fields are applied.²⁷ They also constitute a good example of how to tune the functional properties with respect to different factors, such as the electrical boundary conditions or the periodicity of the superlattice.

On the other hand, the theoretical studies of PbTiO₃/SrTiO₃ superlattices have focused, so far, on three different aspects of the monodomain configurations: (i) the analysis of the structural, electronic, and ferroelectric properties of both the pristine^{28,32,33} and disordered^{32,33} (including the presence of cation intermixing or defects) interfaces, (ii) the study of the coupling between the AFD instabilities and the FE polarization, compatible with an improper ferroelectric behaviour,⁷ or (iii) the influence of strain on the previous coupling.⁸

In this work, we perform first-principles calculations on polydomain phases of (PbTiO₃)_n/(SrTiO₃)_n [($n | n$)] superlattices, with periodicities of $n = 3$ and 6. Our goal is to

gain further insight on the polarization and oxygen octahedra rotation profiles. Besides, we compare the differences in energies between relevant phases. The influence of the periodicity, orientation, energy of the DWs, and the mixed FE-AFD-strain coupling present in these superlattices⁸ are carefully considered. We also analyze the strain fields induced by the domain structure and their role in the interlayer coupling.

The rest of the paper is organized as follows. The method on which the simulations are based is described in Sec. II. In Sec. III A, we compare the energy of the different competing phases (monodomain versus polydomain) to ascertain their relative stability. The atomic structure of the domains is analyzed in Sec. III B. Finally, the polarization profiles and strain fields are discussed in Sec. III C.

II. METHODS

The simulations have been carried out within the local density approximation (LDA) to the density functional theory (DFT) using the SIESTA code.³⁴ The rest of the technical parameters remain the same as in Ref. 8. In this work, we have performed simulations of $(n | n)$ superlattices, by means of a supercell approach. Two values of n have been considered, $n = 3$ and 6 , aiming to sample superlattices within the two distinct regimes experimentally observed: strong (for $n \lesssim 4$) and weak (for $n \gtrsim 4$) electrostatic coupling between the SrTiO₃ and PbTiO₃ layers.

As the starting point, an ideal structure was defined stacking along the [001] direction n unit cells of SrTiO₃ and n unit cells of PbTiO₃. The in-plane lattice constant was fixed to the theoretical LDA value of SrTiO₃ (3.874 Å). First, mirror symmetry planes were imposed at the central atomic layers of PbTiO₃ and SrTiO₃, and an initial atomic relaxation was performed in order to find a reference paraelectric ground state. Then, in order to simulate polydomain configurations with DW running along (010) planes, the reference structure was replicated N_x times along the [100] direction and N_y times along the [010] direction. Due to the periodic boundary conditions used in the simulations, N_x determines the domain periodicity, while N_y allows to switch on ($N_y = 2$) and off ($N_y = 1$) the AFD instabilities. Also DW oriented along the (110) direction have been simulated, using a reference structure with $\sqrt{2} \times \sqrt{2}$ in-plane lattice parameters, which is replicated N_{110} times along the [110] direction for a domain periodicity of $\sqrt{2}N_{110}$. Following the recipe given in Ref. 16, a percentage of the bulk soft mode distortion was superimposed on the PbTiO₃ layers, so the polarization points upwards in half of the superlattice and downward in the other half (positive and negative polarization along the [001] direction, respectively). For $N_y = 2$ superlattices, small rotations were induced by hand following a $a^0 a^0 c^-$ pattern in Glazer notation. Finally, an extra atomic relaxation of the full heterostructure was carried out, until the maximum value of the Hellman-Feynman forces and the zz stress tensor component fell below 0.01 eV/Å and 0.0001 eV/Å³ respectively [except for the (3 | 3) superlattice with $N_x = 16$ and $N_y = 2$ (960 atoms in the simulation box) and for the (6 | 6) superlattice with $N_x = 12$ and $N_y = 1$ (720 atoms), which were relaxed down to a maximum force of 0.05 eV/Å]. To establish the notation, we will call the

plane parallel to the interface the (x, y) plane, whereas the perpendicular direction will be referred to as the z axis.

III. RESULTS

A. Energetics

For the (3 | 3) superlattices, we have performed simulations of the different competing phases in order to determine their relative stability. The energies of the polydomain, monodomain, and nonpolar configurations as a function of the domain periodicity are shown in Fig. 1. For these superlattices, the balance between the electrostatic energy (which tends to reduce the domain period), and the DW energy density (which tends to increase it) results in an optimum periodicity of the domain structure, Λ , of about 12 unit cells (46.5 Å) (the energy for N_x equal 12 and 16 might be considered as equivalent within the accuracy of our simulations).

The most stable phase found in our simulations, however, corresponds to a monodomain structure, with the polarization in the PbTiO₃ layer pointing close to the perovskite unit cell diagonal (configuration described in detail in Ref. 8 and labeled as [111] in Fig. 1). This result is consistent with the upturn in the domain periodicity observed by Zubko and coworkers,³¹ suggesting that for $n < 4$ the superlattices enter into the strong-coupling regime. Nevertheless, the energy difference between the monodomain and the most stable polydomain configuration is very small (of the order of 1.6 meV/five-atom perovskite unit cell, well below the thermal energy at room temperature), suggesting a close competition between them for small values of n . A small change on any external

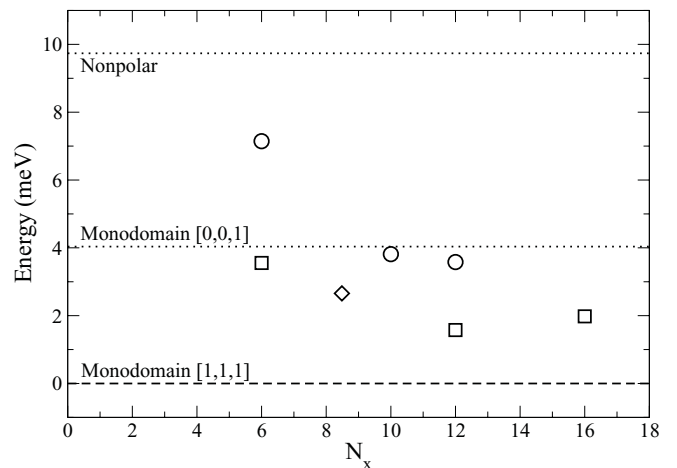


FIG. 1. Differences in energies between polydomain, monodomain, and nonpolar configurations in (3|3) PbTiO₃/SrTiO₃ superlattices, as a function of the domain period N_x . Total energies of supercells are given per five-atom perovskite unit cell. Circles represent the configurations where the AFD modes are not allowed ($N_y = 1$), while squares represent configuration with condensed AFD modes ($N_y = 2$). Diamond indicates a configuration where the DW lies along the (110) direction, also allowing for the condensation of AFD modes. The monodomain phases have been labeled as in Ref. 8, where a full analysis of these configurations is provided. In the nonpolar configuration, the AFD distortions have been considered. All energies are given with respect to the most stable monodomain configuration.

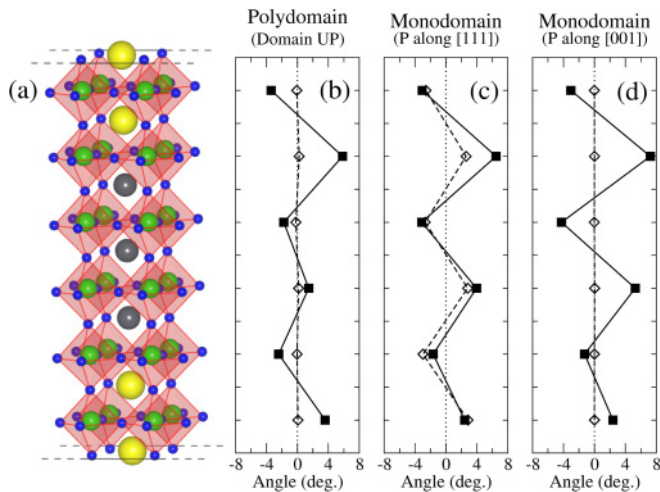


FIG. 2. (Color online) (a) Schematic representation of the center of a domain in a (3|3) $\text{PbTiO}_3/\text{SrTiO}_3$ superlattice (see region embodied by a bracket in Fig. 4). Atoms are represented by balls: Sr in yellow, Ti in green, O in blue, and Pb in grey. In panels (b)–(d) we represent the amplitude of the rotations (squares) and tiltings (diamonds) of each TiO_6 octahedra: (b) at the center of a domain in the polydomain configuration with $N_x = 12$, (c) in the ground state monodomain phase (with polarization in the PbTiO_3 layer pointing close to the perovskite unit cell diagonal, see Ref. 8), and (d) in a monodomain phase with polarization lying along [001].

condition (growth temperature, or how fast the system is cooled, etc.) might help the system to overcome potential energy barriers, activate transitions between them and could, eventually, stabilize a metastable domain structure. This fact might explain why both polydomain and monodomain samples have been observed experimentally.²⁷

For a given domain periodicity, the energy is systematically lowered if the rotation of the oxygen octahedra are allowed, with reductions ranging between 3.6 meV per five-atom perovskite unit cell (for $N_x = 6$) to 2.0 meV (for $N_x = 12$). This highlights the importance of the FE-AFD coupling in these heterostructures. The coupling is also noticeable when the pattern of the oxygen octahedra in the polydomain phases are compared with those of monodomain configuration. We see in Fig. 2 that at the center of the domains (i.e., mid-distance between two DW, see column of atoms embodied by a bracket in Fig. 4) where the polarization is purely out of plane, P_z , the rotations along an in-plane axis (tiltings) essentially vanish, resembling the case of the [001] monodomain phase reported in Ref. 8. Regarding the rotations around the z axis, the larger P_z in the PbTiO_3 layer in polydomain phases penalizes the AFD modes and the rotation angles are smaller. The FE-AFD coupling also affects the magnitude of the polarization, resulting in a slight reduction of P_z when condensation of AFD modes is allowed (see Table I).

We also find that the effect of the DW orientation is small: a change in the orientation of the DW from $\langle 100 \rangle$ to $\langle 110 \rangle$ does not affect significantly the energy of the superlattice. From the energy difference between polydomain configurations with DW running along $\langle 100 \rangle$ and $\langle 110 \rangle$, DW energies of both orientations can be estimated to differ by about 1 mJ/m^2 . This small difference points to a rather isotropic

TABLE I. Out-of-plane polarization, P_z , at the center of the domains in $\text{PbTiO}_3/\text{SrTiO}_3$ superlattices with $N_x = 12$ u.c. P_z^{PTO} (P_z^{STO}) stands for the polarization at the central perovskite unit cell within the PbTiO_3 (SrTiO_3) layer. Values in parenthesis correspond to the rms polarization, averaged along the [100] direction. Units in $\mu\text{C/cm}^2$.

$(n n)$	N_x	N_y	P_z^{PTO}	P_z^{STO}
(3 3)	12	1	65 (56)	31 (26)
(3 3)	12	2	60 (53)	29 (24)
(6 6)	12	1	75 (70)	21 (17)

DW structure, with the energy of the domains depending very weakly on the stripe orientation, in good agreement with experimental results,²⁷ phenomenological Landau-Ginzburg-Devonshire theory,³⁵ and model Hamiltonian¹⁵ simulations.

For the (6 | 6) superlattices, only one domain periodicity was simulated due to the scaling of the computing time with the system size. For the same reason, in this case, rotations of the oxygen octahedra were not allowed in the calculations of the polydomain phases. In view of the results for the (3 | 3) superlattice, we assume that the presence of the octahedra rotations results in a decrease of the energies of polydomains structures and a small reduction of the polarization at the center of the domains. We chose $N_x = 12$ u.c. ($\Lambda = 46.5 \text{ \AA}$), close to the experimental value of $\Lambda = 55 \text{ \AA}$.³⁰ These polydomain phase were found to lie 3.8 meV/five-atom perovskite unit cell below the most stable monodomain phase without AFD.

The change in the most stable phase [from monodomain in the (3 | 3) to polydomain in the (6 | 6)] indicates a crossover between the weak and strong electrostatic coupling regimes described in the introduction. Experimentally, this transition was inferred to occur gradually, with a minimum of the domains size observed at $n \simeq 4$ (see Ref. 31). In related $\text{KTaO}_3/\text{KNbO}_3$ superlattices, the critical periodicity for the crossover ranges between $7 \leq n \leq 15$ (experiments from Ref. 36) and $12 \leq n \leq 24$ (shell models simulations from Ref. 37).

B. Atomic structure of the domains

Figure 3 shows the local polarization profile of the most stable polydomain configurations found for the (3 | 3) and (6 | 6) superlattices (both with a domain periodicity of $N_x = 12$ u.c.). Similar patterns are obtained for other domain sizes. In order to be able to make quantitative comparisons, and since only simulations with $N_y = 1$ are available for the (6 | 6) superlattice, from now on, only simulations where oxygen octahedra were *not* allowed are discussed. The local polarization is obtained calculating the polarization of a unit cell centered on every cation of the system (except at the interfaces where no “bulklike” unit cell can be chosen), and using the displacement of the atoms with respect to the ideal phase and the Born effective charges obtained for the bulk centrosymmetric phase of the corresponding material, either PbTiO_3 or SrTiO_3 , depending on the layer the cation belongs to. Near the DWs the local polarization pattern clearly displays a continuous polarization rotation within 3 u.c. around the DW, connecting two 180° domains.

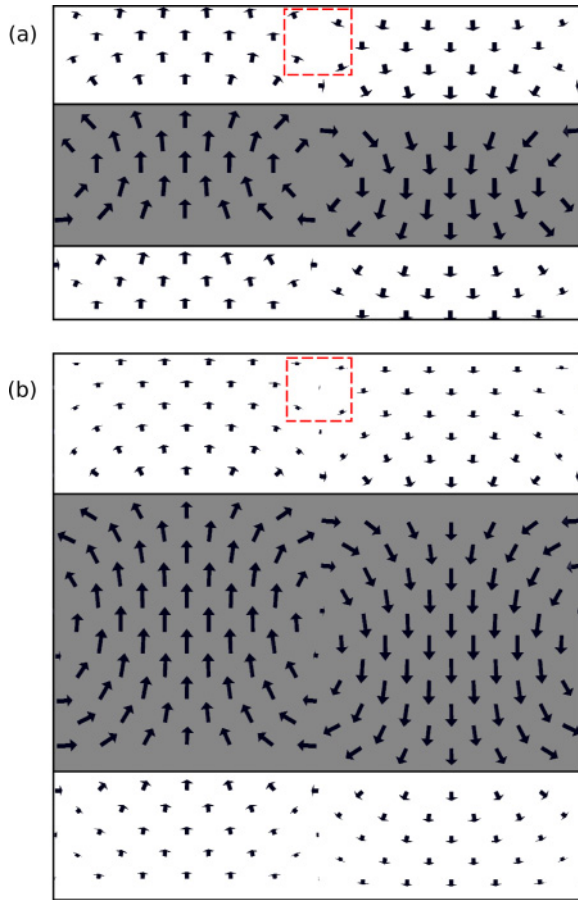


FIG. 3. (Color online) Local polarization profile of polydomain structures in $(\text{PbTiO}_3)_n/(\text{SrTiO}_3)_n$ superlattices with (a) $n = 3$ and (b) $n = 6$. The PbTiO_3 and SrTiO_3 are depicted as gray and white regions respectively. Red dashed squares in the SrTiO_3 layers mark the position where antivortices are formed.

As suggested by the experimental results exposed in Ref. 31, the examination of Fig. 3 reveals that the actual domain structure in this kind of systems is often an intermediate case between 180° domains and the closure domains commonly found in ferromagnets, displaying rotation of the polarization upon approaching the DWs^{14,38} (although the length scale over which the polarization rotation takes place is only a few unit cells in the case of ferroelectrics, in contrast with the several nanometers or even microns typical of ferromagnets). However, we have to keep in mind that in ideal closure domains, the divergence of the polarization vanishes everywhere and, therefore, the depolarizing field is perfectly screened. In our simulations, the polarization of the SrTiO_3 indicates the presence of a residual depolarizing field and thus, strictly speaking, our domains do not constitute perfect domains of closure.

Our results also support the robustness of the rotation of polarization and the formation of vortices in ferroelectric nanostructures suggested by previous theoretical studies. These geometries have been predicted to exist independently of (i) the used methodology (including first principles,^{16,39} model Hamiltonians,⁴⁰⁻⁴² phase field models,⁴³ and phenomenological Devonshire-Ginzburg-Landau theories^{35,44}), and/or

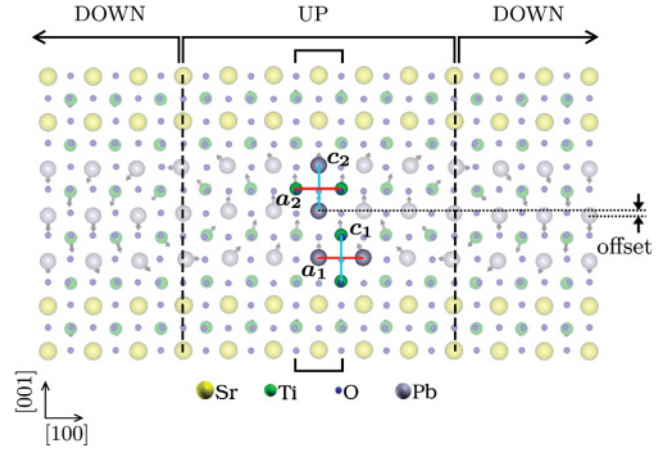


FIG. 4. (Color online) Schematic view of the $(3|3)$ superlattice with $N_x = 12$ and $N_y = 1$ indicating how local values of the magnitudes plotted in Figs. 5 and 7 are defined. Red (blue) lines represent local values of in-plane, a , (out-of-plane, c) lattice constants, measured from the in-plane (out-of-plane) distance between equivalent cations of the same chemical species in consecutive unit cells along the x (z) direction. Magnitudes with subscript 1 (2) indicate unit cells centered on a $[001]$ AO (TiO_2) atomic plane. Local polarization is marked with arrows. Black dotted lines indicate the offset between $[100]$ atomic rows to the left and right of the domain walls, defined as the relative vertical shift of A-cations in a given atomic plane. Bracket at the bottom of the up domain indicates the position of its center, where the values plotted as empty symbols in Figs. 5 and 7 are obtained. Finally, domain walls are represented by dashed lines.

(ii) the electrostatic boundary conditions (with metallic^{16,45} or semiconducting electrodes,^{41,44} or even in free standing slabs^{39,42}).

It is remarkable to see that the polarization rotation in the $\text{PbTiO}_3/\text{SrTiO}_3$ superlattices is mostly due to large in-plane displacement of the Pb atoms at the PbO layers in the vicinity of the interface. This contrasts with the predicted domains in $\text{BaTiO}_3/\text{SrRuO}_3$ capacitors,¹⁶ where the in-plane polarization is due to the displacements of the Sr atoms in the first layer of the electrode. Here, the Pb atoms move of the order of 0.2 \AA , a displacement large enough to be detectable with the recently developed atomic-resolution aberration-corrected transmission electron microscopy. Using this technique, polarization rotation at DWs have been experimentally observed in ferroelectric thin films with thicknesses of a few tens of unit cells.^{19,20} However the high quality level achieved during the last years in the growth of short-period superlattices, together with the large in-plane displacements predicted, make this kind of system particularly suited for the observation of the formation of vortices at domain walls in ultrathin films, comparable in size to the simulated systems listed above.

Interestingly, within the SrTiO_3 layer and close to the DW, we do observe the formation of antivortices; a local polarization pattern where two dipoles point face to face and two tail to tail (see red dashed squares in Fig. 3). (These antivortices have also been recently predicted to form in epitaxial BiFeO_3 films.⁴⁶)

C. Polarization profiles and strain field

Within a polydomain configuration, there is no longer any need to maintain the normal component of the polarization at the interface, P_z , constant, since the electric fields that arise from its discontinuity are efficiently screened by the presence of domains. As a consequence P_z , that in the monodomain configuration is continuous throughout the superlattice, in the polydomain case is very inhomogeneous with polarization mismatches at the center of the domains of $34 \mu\text{C}/\text{cm}^2$ and $54 \mu\text{C}/\text{cm}^2$ for the (3 | 3) and (6 | 6) superlattice, respectively (see Table I).

The layer-by-layer polarization of Figs. 5(a) and 5(c) shows that, within SrTiO₃, it converges to a rather homogeneous well defined value, that at the center of the domain decreases from $31 \mu\text{C}/\text{cm}^2$ (for $n = 3$) to $21 \mu\text{C}/\text{cm}^2$ (for $n = 6$). On the contrary, the PbTiO₃ layer displays a smooth variation of the polarization, with a progressive reduction spanning over a length of three unit cells into the PbTiO₃ layers from the interface. The great reduction of the polarization of the SrTiO₃ layer upon a increase in n , together with the out-of-plane polarization at the center of the PbTiO₃ layer rapidly approaching the bulk value ($83 \mu\text{C}/\text{cm}^2$), again supports the gradual electrostatic decoupling of the ferroelectric layer.³¹

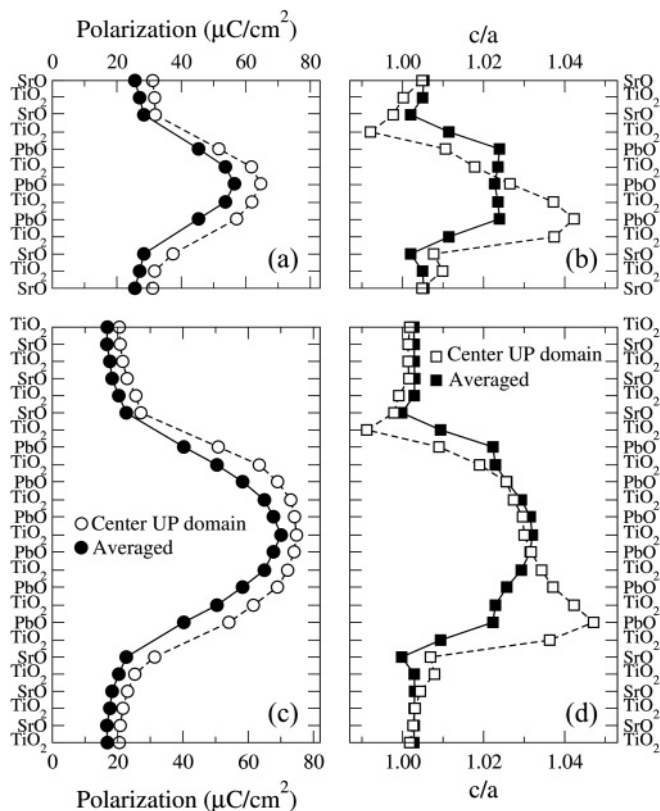


FIG. 5. Left panels: layer-by-layer out-of-plane polarization, P_z , inferred from the Born effective charges and the atomic displacements for (a) a (3 | 3) and (c) a (6 | 6) superlattice. Right panels: layer-by-layer tetragonality for (b) a (3 | 3) and (d) a (6 | 6) superlattice. Empty symbols represent values at the center of an up domain, while filled symbols correspond to averaged values (root mean square in the case of polarization) along the [100] direction.

In Fig. 5, we also plot the variation of the local tetragonality across the superlattice, calculated for the same perovskite unit cell surrounding each cation. The layer-by-layer tetragonality averaged along the [100] direction, plotted as black squares in Figs. 5(b) and 5(d), displays a variation that is well correlated with that of the polarization: an almost constant value inside the SrTiO₃ layer and a smooth increase from the interfaces toward the center of the PbTiO₃. The polarization of the SrTiO₃ layer induces a slight tetragonality of this material. This reduction of symmetry with respect to the cubic unit cell of bulk SrTiO₃ is consistent with the decrease of the $t_{2g}-e_g$ splitting observed in the EELS spectra of this system by Zubko and coworkers.³¹

Besides, in Figs. 5(b) and 5(d), we show the layer-by-layer tetragonality across the superlattice at the center of a domain with the polarization pointing up. Strikingly, and contrary to the polarization, the variation of the local tetragonality as we move across the superlattice is very asymmetric. The tetragonality reaches its maximum value in the PbTiO₃ layer at the bottom interface with respect to the polarization direction, and gradually reduces its magnitude as we move toward the top interface. In the SrTiO₃ layer, the strain gradient is smaller and forced by the imposed periodic boundary conditions, it has opposite sign.

The analysis of the polarization and tetragonality profiles reveals that the formation of domains in the superlattices is associated with complex distortions. The characteristics of the strain field in this system can be explained as a combination of different effects.

On the one hand, in PbTiO₃ the off-center displacements of both the Pb and Ti cations contribute to the polarization. Therefore the Pb atoms displace along z in opposite direction in the up and down domains. This gives rise to an *offset* between [100] atomic rows to the left and right of the DW [see Fig. 6(a)]. A sizable offset of 0.6 Å was already predicted by Meyer and Vanderbilt in 180° stripe domains in bulk PbTiO₃.⁴⁷ As in Ref. 47, for the PbTiO₃/SrTiO₃ superlattices we quantify this offset for a given layer as the difference in the z coordinate of a equivalent A cation at the center of opposite domains (see Fig. 4). The layer by layer offset, shown in Figs. 7(a)

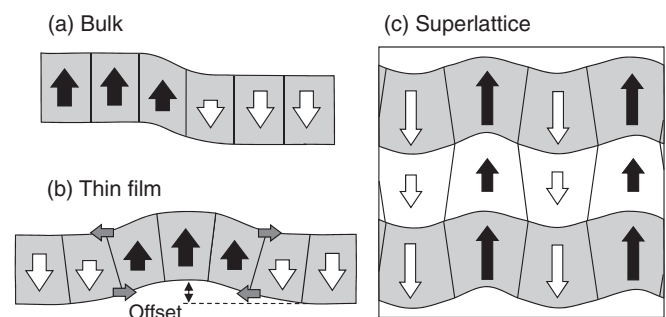


FIG. 6. Schematic representation of the distortion induced by the domain structure in (a) bulk PbTiO₃, (b) PbTiO₃ thin films and (c) PbTiO₃/SrTiO₃ superlattices. (a) In bulk, displacements of Pb cations cause an offset between [100] atomic rows across the DW. (b) In thin films, in addition to the offset between domains, rotation of the polarization near the interface is responsible of a nonvanishing strain gradient $\frac{\partial \epsilon_{11}}{\partial z}$. (c) In the case of the PbTiO₃/SrTiO₃ superlattices, the offset and modulation of the strain field in the PbTiO₃ layer (in grey) propagates into the SrTiO₃ (in white).

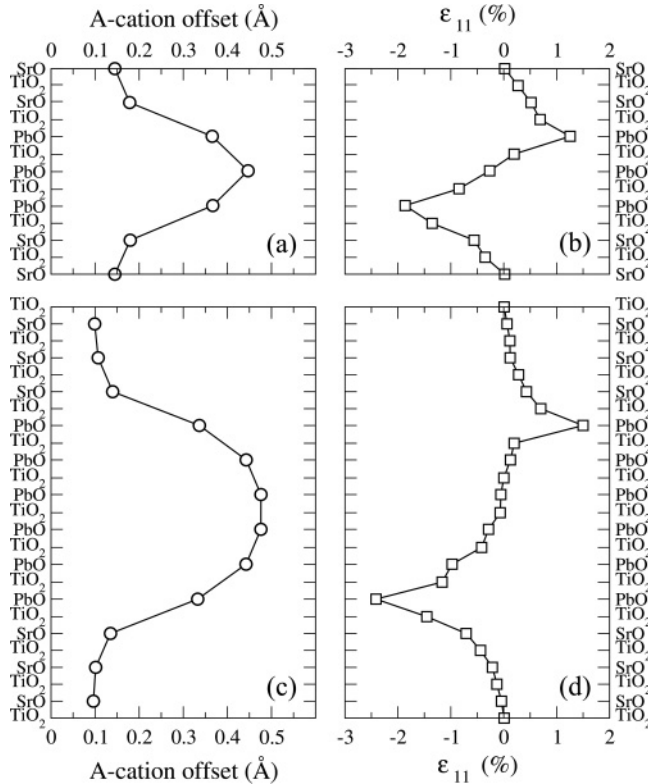


FIG. 7. Left panels: local layer-by-layer offset between [100] atomic rows to the left and right of the DW for (a) a (3 | 3) and (c) a (6 | 6) superlattice. Right panels: local in-plane strain across the center of an up domain in (b) a (3 | 3) and (d) a (6 | 6) superlattice. A large nondiagonal component of the strain gradient, $\frac{\partial \epsilon_{11}}{\partial z}$ can be observed close to the interfaces.

and 7(c), amounts up to almost 0.5 (0.45) Å at the middle of the PbTiO₃ layer in the (6 | 6) [(3 | 3)] superlattice. Although the offset of opposite domains is partially accommodated by the interfaces—which reflects in the increase (decrease) of the tetragonality at the bottom (top) interface in Figs. 5(b) and 5(d)—it still propagates into the SrTiO₃, amounting a sizable ~ 0.1 Å.

On the other hand, in thin films the polarization in PbTiO₃ rotates at the DW. Indeed, as pointed out above, our simulations show that large in-plane displacements of the Pb atoms (up to 0.2 Å) take place at the interfaces. It is sensible to argue that this in-plane polarization is coupled with an in-plane strain and, as it is schematically depicted in Fig. 6(b), it pushes the DW in the same direction of the polarization. This effect is reinforced as consecutive DWs become closer, as it happens in ferroelectric thin films [see Fig. 6(b)]. As a consequence, the in-plane lattice constant is expected to be enlarged at the top interface (with respect to polarization direction) and compressed at the bottom interface. To test this hypothesis we have performed a detailed analysis of the strain field in the system, calculating for every individual perovskite unit cell the local values of the in-plane lattice constant, a (see Fig. 4 for an explanation about how it is computed). The local in-plane strain, calculated as $\epsilon_{11} = a/a_0 - 1$, where $a_0 = a_{\text{SrTiO}_3} = 3.874$ Å is plotted in Figs. 7(b) and 7(d) for the (3 | 3) and (6 | 6) superlattices, respectively. It shows a

variation with respect to the position along the z direction that can be clearly correlated with that of the tetragonality, shown in Figs. 5(b) and 5(d): PbTiO₃ unit cells close to the bottom interface (with respect to the polarization direction) are compressed in-plane, and as a result, they tend to elongate along the z axis. Conversely, at the top interface, the material is expanded in-plane and presents a reduced tetragonality. Since the in-plane polarization is confined at the interfaces, large strain gradients $\partial \epsilon_{11} / \partial z$ can be anticipated. In fact, huge values are obtained from our simulations: up to $4 \times 10^7 \text{ m}^{-1}$, more than seven orders of magnitude larger than those obtained in bending experiments on SrTiO₃.⁴⁸ Similar distortions are found in the SrTiO₃ layer, although with opposite sign of the strain gradients.

Finally, in the superlattice, the SrTiO₃ atomic layers closer to the interface are forced to follow the local in plane expansion or contraction of the PbTiO₃ [see Fig. 6(c)]. However, the presence of an inhomogeneous strain in the SrTiO₃ is energetically very costly. Therefore it rapidly recovers a nearly constant in-plane lattice parameter [see Fig. 7(d)].

The combined effect of the domain offset and the modulation of the strain field can explain the large out-of-plane coherence length of domain structure previously observed in this superlattice.³¹ Even for relatively large thicknesses of SrTiO₃ for which the ferroelectric layers can be considered as being electrostatically decoupled, domains with the same orientation of the polarization are aligned along the [001] direction.

The large strain gradients associated with the polydomain configurations might, in addition, significantly affect the local polarization pattern through the flexoelectric effect.^{49–53} A numerical quantification of the corresponding nondiagonal component of the flexoelectric tensor is extremely subtle, since it might be hidden by strain contributions via piezoelectric effects, and is out of the scope of this paper. However, assuming a flexoelectric coefficient of the order of 1 nC/m (typical of ferroelectric perovskites⁴⁸) and with the strain gradients extracted above, we estimate that the flexoelectric-induced polarization can reach values of a few $\mu\text{C}/\text{cm}^2$ at the interfaces or at the center of the short period superlattices.

IV. CONCLUSIONS

In summary, using accurate first-principles simulations we have studied the domain structures in short-period (PbTiO₃) _{n} /(SrTiO₃) _{n} superlattices. The most important conclusions that can be drawn follow. (i) The domain structures might compete in energy with monodomain configurations. (ii) The domains are rather isotropic, a change in the orientation of the DW from $\langle 100 \rangle$ to $\langle 110 \rangle$ does not affect significantly the energy of the superlattice. (iii) From the structural point of view, they display polarization rotation, similar to the one theoretically predicted in ferroelectric nanocapacitors and recently observed in various ferroelectric ultrathin films. (iv) Our results suggest the progressive transition as a function of n from a strongly electrostatic coupled regime (where the ground state is a monodomain configuration with a constant out-of-plane component of the polarization preserved throughout the structure) to a weakly coupled regime (where the polarization is confined within the PbTiO₃ layers forming

domains). (v) The evolution of the out-of-plane layer-by-layer polarization and tetragonality within the SrTiO₃ and the PbTiO₃ layers are consistent with the t_{2g} - e_g splitting inferred from the unit-cell resolution recently measured by EELS experiments.³¹ (vi) Large offsets between [100] atomic rows across the DW and huge strain gradients (seven orders of magnitude larger than those obtained in bending experiments on SrTiO₃⁴⁸) are observed. The contribution of both of them can be responsible of the out-of-plane coherence of the domain structure found experimentally.³¹ This study should complement experimental studies and could guide the design of new artificial structures with even more appealing functionalities.

ACKNOWLEDGMENTS

The authors thank P. Zubko for the valuable discussion and his careful reading of the manuscript. This work was supported by the Spanish Ministry of Science and Innovation through the MICINN Grant FIS2009-12721-C04-02, by the Spanish Ministry of Education through the FPU fellowship AP2006-02958 (PAP), and by the European Union through the project EC-FP7, Grant No. CP-FP 228989-2 “OxIDes.” The authors thankfully acknowledge the computer resources, technical expertise, and assistance provided by the Red Española de Supercomputación. Calculations were also performed at the ATC group of the University of Cantabria.

-
- ¹M. Dawber, K. M. Rabe, and J. F. Scott, *Rev. Mod. Phys.* **77**, 1083 (2005).
- ²Ph. Ghosez and J. Junquera, *Handbook of Theoretical and Computational Nanotechnology*, edited by M. Rieth and W. Schommers, Vol. 9 (American Scientific Publishers, Stevenson Ranch, CA, 2006), pp. 623–728.
- ³P. Zubko, S. Gariglio, M. Gabay, Ph. Ghosez, and J. M. Triscone, *Annu. Rev. Condens. Matter Phys.* **2**, 141 (2011).
- ⁴J. B. Neaton and K. M. Rabe, *Appl. Phys. Lett.* **82**, 1586 (2003).
- ⁵S. M. Nakhmanson, K. M. Rabe, and D. Vanderbilt, *Appl. Phys. Lett.* **87**, 102906 (2005).
- ⁶D. G. Schlom, L. Q. Chen, C. B. Eom, K. M. Rabe, S. K. Streiffer, and J. M. Triscone, *Annu. Rev. Mater. Res.* **37**, 589 (2007).
- ⁷E. Bousquet, M. Dawber, N. Stucki, C. Lichtensteiger, P. Hermet, S. Gariglio, J. M. Triscone, and Ph. Ghosez, *Nature (London)* **452**, 732 (2008).
- ⁸P. Aguado-Puente, P. García-Fernández, and J. Junquera, *Phys. Rev. Lett.* **107**, 217601 (2011).
- ⁹N. A. Benedek and C. J. Fennie, *Phys. Rev. Lett.* **106**, 107204 (2011).
- ¹⁰J. M. Rondinelli and N. A. Spaldin, *Adv. Mater.* **23**, 3363 (2011).
- ¹¹J. Seidel, L. W. Martin, Q. He, Q. Zhan, Y. H. Chu, A. Rother, M. E. Hawkrige, P. Maksymovych, P. Yu, M. Gajek, N. Balke, S. V. Kalinin, S. Gemming, F. Wang, G. Catalan, J. F. Scott, N. A. Spaldin, J. Orenstein, and R. Ramesh, *Nat. Mater.* **8**, 229 (2009).
- ¹²J. Guyonnet, I. Gaponenko, S. Gariglio, and P. Paruch, *Adv. Mater.* **23**, 5377 (2011).
- ¹³G. Catalan, A. Janssens, G. Rispens, S. Csiszar, O. Seeck, G. Rijnders, D. H. A. Blank, and B. Noheda, *Phys. Rev. Lett.* **96**, 127602 (2006).
- ¹⁴D. Lee, R. K. Behera, P. Wu, H. Xu, Y. L. Li, S. B. Sinnott, S. R. Phillpot, L. Q. Chen, and V. Gopalan, *Phys. Rev. B* **80**, 060102 (2009).
- ¹⁵B.-K. Lai, I. Ponomareva, I. A. Kornev, L. Bellaiche, and G. J. Salamo, *Phys. Rev. B* **75**, 085412 (2007).
- ¹⁶P. Aguado-Puente and J. Junquera, *Phys. Rev. Lett.* **100**, 177601 (2008).
- ¹⁷S. Prosandeev, S. Lisenkov, and L. Bellaiche, *Phys. Rev. Lett.* **105**, 147603 (2010).
- ¹⁸Y. Ivry, D. P. Chu, J. F. Scott, and C. Durkan, *Phys. Rev. Lett.* **104**, 207602 (2010).
- ¹⁹C.-L. Jia, K. W. Urban, M. Alexe, D. Hesse, and I. Vrejoiu, *Science* **331**, 1420 (2011).
- ²⁰C. T. Nelson, B. Wincheser, Y. Zhang, S.-J. Kim, A. Melville, C. Adamo, C. M. Folkman, S. H. Baek, C. B. Eom, D. G. Schlom, L.-Q. Chen, and X. Pan, *Nano Lett.* **11**, 828 (2011).
- ²¹I. I. Naumov, L. Bellaiche, and H. X. Fu, *Nature (London)* **432**, 737 (2004).
- ²²S. Prosandeev, I. Ponomareva, I. Naumov, I. Kornev, and L. Bellaiche, *J. Phys.: Condens. Matter* **20**, 193201 (2008).
- ²³S. K. Streiffer, J. A. Eastman, D. D. Fong, C. Thompson, A. Munkholm, M. V. Ramana Murty, O. Auciello, G. R. Bai, and G. B. Stephenson, *Phys. Rev. Lett.* **89**, 067601 (2002).
- ²⁴G. B. Stephenson, D. D. Fong, M. V. R. Murty, S. K. Streiffer, J. A. Eastman, O. Auciello, P. H. Fuoss, A. Munkholm, M. E. M. Aanerud, and C. Thompson, *Physica B* **336**, 81 (2003).
- ²⁵D. D. Fong, G. B. Stephenson, S. K. Streiffer, J. A. Eastman, O. Auciello, P. H. Fuoss, and C. Thomson, *Science* **304**, 1650 (2004).
- ²⁶C. Thompson, D. D. Fong, R. V. Wang, F. Jiang, S. K. Streiffer, K. Latifi, J. A. Eastman, P. H. Fuoss, and G. B. Stephenson, *Appl. Phys. Lett.* **93**, 182901 (2008).
- ²⁷P. Zubko, N. Stucki, C. Lichtensteiger, and J.-M. Triscone, *Phys. Rev. Lett.* **104**, 187601 (2010).
- ²⁸M. Dawber, C. Lichtensteiger, M. Cantoni, M. Veithen, Ph. Ghosez, K. Johnston, K. M. Rabe, and J. M. Triscone, *Phys. Rev. Lett.* **95**, 177601 (2005).
- ²⁹J. Y. Jo, P. Chen, R. J. Sichel, S. J. Callori, J. Sinsheimer, E. M. Dufresne, M. Dawber, and P. G. Evans, *Phys. Rev. Lett.* **107**, 055501 (2011).
- ³⁰A. Torres-Pardo, A. Gloter, P. Zubko, N. Jecklin, C. Lichtensteiger, C. Colliex, J.-M. Triscone, and O. Stéphan, *Phys. Rev. B* **84**, 220102 (2011).
- ³¹P. Zubko, N. Jecklin, A. Torres-Pardo, P. Aguado-Puente, A. Gloter, C. Lichtensteiger, J. Junquera, O. Stéphan, and J.-M. Triscone (accepted for publication in *Nano Lett.*, 2012).
- ³²V. R. Cooper, K. Johnston, and K. M. Rabe, *Phys. Rev. B* **76**, 020103(R) (2007).
- ³³M. Gu, J. Wang, Q. Y. Xie, and X. S. Wu, *Phys. Rev. B* **82**, 134102 (2010).
- ³⁴J. M. Soler, E. Artacho, J. D. Gale, A. García, J. Junquera, P. Ordejón, and D. Sánchez-Portal, *J. Phys.: Condens. Matter* **14**, 2745 (2002).
- ³⁵A. M. Bratkovsky and A. P. Levanyuk, *Phys. Rev. B* **84**, 045401 (2011).

- ³⁶E. D. Specht, H. M. Christen, D. P. Norton, and L. A. Boatner, *Phys. Rev. Lett.* **80**, 4317 (1998).
- ³⁷M. Sepliarsky, S. R. Phillpot, D. Wolf, M. G. Stachiotti, and R. L. Mignoni, *Phys. Rev. B* **64**, 060101(R) (2001).
- ³⁸C. Kittel, *Phys. Rev.* **70**, 965 (1946).
- ³⁹T. Shimada, S. Tomoda, and T. Kitamura, *Phys. Rev. B* **81**, 144116 (2010).
- ⁴⁰B.-K. Lai, I. Ponomareva, I. I. Naumov, I. A. Kornev, H. Fu, L. Bellaiche, and G. J. Salamo, *Phys. Rev. Lett.* **96**, 137602 (2006).
- ⁴¹S. Prosandeev and L. Bellaiche, *Phys. Rev. B* **75**, 172109 (2007).
- ⁴²D. Sichuga and L. Bellaiche, *Phys. Rev. Lett.* **106**, 196102 (2011).
- ⁴³J. Slutsker, A. Artemev, and A. Roytburd, *Phys. Rev. Lett.* **100**, 087602 (2008).
- ⁴⁴G. B. Stephenson and K. R. Elder, *J. Appl. Phys.* **100**, 051601 (2006).
- ⁴⁵C. Lichtensteiger, P. Zubko, M. Stengel, P. Aguado-Puente, J. M. Triscone, Ph. Ghosez, and J. Junquera, in *Oxide Ultrathin Films: Science and Technology*, edited by G. Pacchioni and S. Valeri (Wiley, 2011).
- ⁴⁶S. Prosandeev, I. A. Kornev, and L. Bellaiche, *Phys. Rev. Lett.* **107**, 117602 (2011).
- ⁴⁷B. Meyer and D. Vanderbilt, *Phys. Rev. B* **65**, 104111 (2002).
- ⁴⁸P. Zubko, G. Catalan, P. R. L. Welche, A. Buckley, and J. F. Scott, *Phys. Rev. Lett.* **99**, 167601 (2007).
- ⁴⁹L. E. Cross, *J. Mater. Sci.* **41**, 53 (2006).
- ⁵⁰J. Hong, G. Catalan, J. F. Scott, and E. Artacho, *J. Phys.: Condens. Matter* **22**, 112201 (2010).
- ⁵¹G. Catalan, A. Lubk, A. H. G. Vlooswijk, E. Snoeck, C. Magen, A. Janssens, G. Rispens, G. Rijnders, D. H. A. Blank, and B. Noheda, *Nat. Mater.* **10**, 963 (2011).
- ⁵²D. Lee, A. Yoon, S. Y. Jang, J.-G. Yoon, J.-S. Chung, M. Kim, J. F. Scott, and T. W. Noh, *Phys. Rev. Lett.* **107**, 057602 (2011).
- ⁵³J. Hong and D. Vanderbilt, *Phys. Rev. B* **84**, 180101(R) (2011).
- ⁵⁴E. V. Bursian and O. I. Zaikovskii, *Sov. Phys. Solid State* **10**, 1121 (1968).
- ⁵⁵E. V. Bursian, *Ferroelectrics* **307**, 177 (2004).